Photochemistry and Photobiology, 2023, 99: 1218–1224

Research Article

Engineered Ferritin with Eu^{3+} as a Bright Nanovector: A Photoluminescence Study

Luisa Affatigato[1], Alice Sciortino*[1], Giuseppe Sancataldo[1], Alessio Incocciati[2], Roberta Piacentini[2], Alessandra Bonamore*[2], Marco Cannas[1], Fabrizio Messina[1], Mariano Licciardi[3] and Valeria Militello[1]

[1]Department of Physics and Chemistry – Emilio Segrè, University of Palermo, Palermo, Italy
[2]Department of Biochemistry – A. Rossi Fanelli, Sapienza University, Rome, Italy
[3]Department of Biological, Chemical and Pharmaceutical Sciences and Technologies (STEBICEF), University of Palermo, Palermo, Italy

Received 5 August 2022, accepted 6 December 2022, DOI: 10.1111/php.13759

ABSTRACT

Ferritin nanoparticles play many important roles in theranostic and bioengineering applications and have been successfully used as nanovectors for the targeted delivery of drugs due to their ability to specifically bind the transferrin receptor (TfR1, or CD71). They can be either genetically or chemically modified for encapsulating therapeutics or probes in their inner cavity. Here, we analyzed a new engineered ferritin nanoparticle, made of the H chain mouse ferritin (HFt) fused with a specific lanthanide binding tag (LBT). The HFt-LBT has one high affinity lanthanide binding site per each of the 24 subunits and a tryptophane residue within the tag that acts as an antenna able to transfer the energy to the lanthanide ions *via* a LRET process. In this study, among lanthanides, we selected europium for its red emission that allows to reduce overlap with tissue auto-fluorescence. Steady state emission measurements and time-resolved emission spectroscopy have been employed to investigate the interaction between the HFt-LBT and the Eu^{3+} ions. This allowed us to identify the Eu^{3+} energy states involved in the process and to pave the way for the future use of HFt-LBT Eu^{3+} complex in theranostics.

INTRODUCTION

One of the major challenges for the prospective use of nanomaterials in cancer theranostics is the development of nanoplatforms capable of targeting cancer cells with high sensitivity and specificity. Ferritin H-homopolymers have been extensively studied as nanocarriers which can be applied as imaging agents (1) or as nanovectors for the targeted delivery of drugs (2–6) due to their ability to bind the transferrin receptor (TfR1 or CD71), highly overexpressed in most tumor cells (7,8). TfR1 is one of the most attractive cancer targets, since tumor cells express up to 100 fold higher levels of TfR1 with respect to healthy cells, and actively internalize the H-Ferritin:TfR1 ligand-receptor complex, in order to accumulate the large amounts of iron required for unrestrained cell growth (9,10). Recent studies, carried out *in vivo* using paramagnetic ferritins within the context of MRI investigations in tumor models, demonstrated that H-ferritin nanoparticles can distinguish cancerous cells from normal cells with a sensitivity of 98% and a specificity of 95% (11).

Ferritin is a cage-like protein made of 24 subunits with an outer diameter of 12 nm and an inner diameter of 8 nm (12,13). Ferritins are ubiquitous and well-characterized iron storage and detoxification proteins. In bacteria and plants, ferritins are homopolymers composed of H-type subunits, while in vertebrates, ferritins typically consist of 24 subunits of two different types, H and L. The H-subunit is responsible for the rapid oxidation of Fe(II) to Fe(III) and for binding the TfR1 receptor, whereas the L-subunit appears to help iron clearance from the ferroxidase centre of the H-subunit and support iron nucleation and mineralization (14,15). The symmetrical positioning of three or four subunits in the protein shell results in the formation of the 3-fold channels and the 4-fold channels respectively. The former are hydrophilic channels connecting the inner cavity to the outside and allows the entry and exit of iron and other cations with a high selectivity (16).

Besides their physiological function, the nanocage properties of ferritins have been investigated in several different biotechnological applications, such as drug delivery vectors (2,16), scaffolds for vaccine development (17) and tools for bioimaging (18,19). Concerning these tools, many studies have been carried out on quantum dots, gold nanoparticles and luminescent metal chelators (20,21), whereas only a few studies have been done on ferritin-based constructs to use as smart luminescent probes. However, advanced optical imaging techniques need an expanded color palette of bright luminescent probes for biological visualization in order to enable real-time cellular imaging with high spatial resolution for close-up view into subcellular compartments, while providing consistent reduction of autofluorescence from biological specimen. In this framework, time delayed luminescence imaging techniques represent the key tool in order to achieve high resolution and low background intensity (22–26).

In this work, an engineered H-ferritin nanoparticle carrying a lanthanide binding tag at the C-terminal end of each subunit

*Corresponding authors email: alice.sciortino02@unipa.it (Alice Sciortino), email: alessandra.bonamore@uniroma1.it (Alessandra Bonamore)

(HFt-LBT) has been characterized for its interaction with europium ions (Eu^{3+}) in view of potential applications in bioimaging. Luminescent probes based on trivalent lanthanide ions are becoming widespread due to their advantageous photophysical properties (22,23): narrow band emission spectra, large Stokes shift (150–300 nm), and long luminescence lifetimes from micro to milliseconds (24,25). Lanthanide f-electrons can radiate most of the absorbed energy, but their small absorption cross sections hamper their practical use (26). Lanthanides are usually not excited by direct light irradiation within their absorption peak, but rather excited through small organic fluorophores, that absorb in the UV region with an adequate absorption cross section and transfer the absorbed energy to the lanthanide atom (27,28). Such a luminescence resonance energy transfer (LRET) strongly depends on the proximity between the two fluorophores (29,30) and can also be used as a probe of the local geometry around the lanthanide site.

Among lanthanides, Eu^{3+} ions are of strong interest in many photonic applications (31,32), in particular in organic light emitting diodes (OLEDs), lasers, optical communications, chemical sensor (33). Eu^{3+} is particularly suitable for bioimaging because its red emission allows to reduce overlap with tissue autofluorescence and to match the biological transparency window. Besides, the fine structure and the relative intensities of Eu^{3+} optical transitions depend on the local environmental conditions, so that they can be used for nanosensing applications.

To the purposes of this work, we have used the H chain mouse ferritin fused with a lanthanide binding tag (LBT) on its C-terminal end to facilitate the incorporation of Eu^{3+} ions into the ferritin nanoparticle. The LBT is a stretch of 17 aminoacids (YIDTNNDGWIEGDELLA) endowed with strong luminescence resonance energy transfer (LRET) sensitization properties since it has a tryptophan (Trp) residue that can act as an antenna transferring the absorbed energy to the lanthanide ion. Furthermore, the LBT shows low nanomolar affinities for the target ions and selectively binds to lanthanides as compared to over other common metal ions (34). LBT is the most convenient option for lanthanide protein labelling in that it can be directly encoded within a recombinant protein expression construct. The tag has been designed to be located inside the inner cavity, so the lanthanide ions diffusing through the surface pores could bind to the LBT sequence (Fig. 1).

The construct would thus act both as carrier targeted to CD71 receptors and as a LRET sensitizer. Mouse ferritin was used in view of the identical sequence within the CD71 binding region as the human ferritin sequence and because of obviously more favorable immunogenic profile for forthcoming *in vivo* study in mouse.

Here we studied the interaction between the Eu^{3+} ions and the HFt-LBT by means of spectroscopic techniques, in order to investigate the interaction between the protein and the lanthanide ions and to pave the way to the future use of HFt-LBT Eu^{3+} complex in theranostics. Steady state emission measurements clearly show the interaction between them by the huge increase of Eu^{3+} emission due to an energy transfer from the Trp to the ions. Time-resolved emission spectroscopy has been employed to deeply investigate this energy transfer and allows us to discriminate the presence of two Eu^{3+} species: one bonded on the LBT and one located in the other sites of the HFt-LBT. Moreover, we have been able to identify the Eu^{3+} energy states involved in the process, which provides evidence to attribute the LRET process to a multipolar energy transfer which prevails on FRET or Dexter-type processes.

MATERIALS AND METHODS

Protein expression and purification. Mouse H ferritin fused with a lanthanide binding tag (HFt-LBT) was expressed in *Escherichia coli* BL21 upon induction with 1 mM IPTG (Isopropyl-β-D-1-thiogalactopyranoside) at OD_{600} = 0.6 for 16 h. Bacterial paste from 2 L culture was resuspended and sonicated in 100 mL of 20 mM HEPES buffer, pH 7.5, containing 200 mM NaCl, 1 mM TCEP (tris(2-carboxiethyl)phosphine), and protease inhibitors. The supernatant was heated at 78°C for 10 min and the denatured proteins were removed by centrifugation. The soluble fraction was treated with 50% and 70% $(NH_4)_2SO_4$ and both the pellets were resuspended in 20 mM sodium phosphate buffer pH 7.2 containing 20 mM $MgCl_2$, extensively dialyzed *versus* the same buffer, and then digested with 5 mg of deoxyribonuclease I for 1 h at 37°C. After digestion, the protein sample was dialyzed *versus* 20 mM HEPES buffer pH 7.4 containing 150 mM NaCl and loaded onto a HiLoad 26/600 Superdex 200 pg column previously equilibrated in the same buffer, using an ÄKTA-Pure apparatus (Cytiva). The eluted ferritin was concentrated using Amicon Ultra-15 centrifugal filter devices (100 kDa cut-off), sterile filtered, and stored at 4°C. Protein concentration was calculated by measuring the UV spectrum using an extinction coefficient of 32 400 M^{-1} cm^{-1} and protein purity was checked by SDS-PAGE. Protein yield was about 50 mg per 1 L culture.

Photoluminescence of HFt-LBT Eu^{3+}. Intrinsic luminescence emission spectra were detected using a Jasco FP-6500 equipped with a Jasco peltier thermostat; samples were positioned in a quartz cuvette of 1 cm and all emission spectra were recorded at 0.5 nm wavelength intervals with excitation and emission bandwidth of 10 nm, scan speed of 100 nm min^{-1} and integration time of 1 s upon excitation at 280 nm at 25°C. Luminescence static spectra were performed using 10 μM HFt-LBT in 3 mL HEPES 20 mM and NaCl 150 mM buffer solution pH 6.4. Luminescence spectra of the protein Eu^{3+} complexes were recorded after 30 min incubation and after addition of incremental amount of $EuCl_3$ in buffer solution in order to saturate all possible Eu^{3+} binding sites in HFt-LBT. Before recording spectra, protein solutions were exchanged with buffer (europium free) by doing dialysis using a molecular porous membrane tubing MWCO: 3.5 kD (Spectral/Por Dialysis Membrane Standard RC Tubing) in order to remove unbound and weakly bound metal ions (four exchanges steps). Protein concentration was measured again and adjusted to the final concentration with buffer. Luminescence titrations were carried out by adding in the sample incremental amount (5 μL or multiples) of a 3 mM europium stock solution under stirring. Emission spectra were recorded 30 min after addition of $EuCl_3$ solution aliquots. Luminescence intensity of Hft-LBT Eu^{3+} complex as a function of the Eu^{3+}/HFt-LBT ratio has been reported. Luminescence intensity was recorded at 615 nm and 329 nm corrected for the dilution factor.

Time-resolved photoluminescence of HFt-LBT Eu^{3+}. Time-resolved photoluminescence decays were recorded using 10 μM HFt-LBT in 3 mL HEPES 20 mM and NaCl 150 mM buffer solution pH 6.4 with different concentrations of Eu^{3+}. The emission spectra were recorded by exciting the samples by 5 ns laser pulses (IRF ~2 ns) of 0.1–0.2 mJ energy derived from a tunable laser (410–700 nm) consisting of an OPO (optical parametric oscillator) pumped by the third harmonic of a pulsed Q-switched Nd:YAG laser and finally duplicated by an UV-module in order to obtain 280 nm nanosecond beam. The spectra and the kinetics were detected by an intensified CCD camera which acquires the emission spectra within a specific time frame (the duration can be set by the operator), with controlled delays with respect to the laser pulse. The time frame is fixed at 20 ms with zero delay from the laser pulse in order to obtain an equivalent of a steady state measurement. In this way, the whole emission is collected. The appropriate time frame was set on the basis of the expected lifetime of the sample we wanted to collect. Thus far, a temporal window of 0.5 ns was set to record short lifetimes such as the one of the Trp, and a time frame of 25 μs and 100 μs to record the europium longer lifetimes. The Eu^{3+} emission decay profiles were least-squares fitted to a biexponential fitting function $I(t) = A_1\exp\left\{-\frac{t}{\tau_1}\right\} + A_2\exp\left\{-\frac{t}{\tau_2}\right\}$.

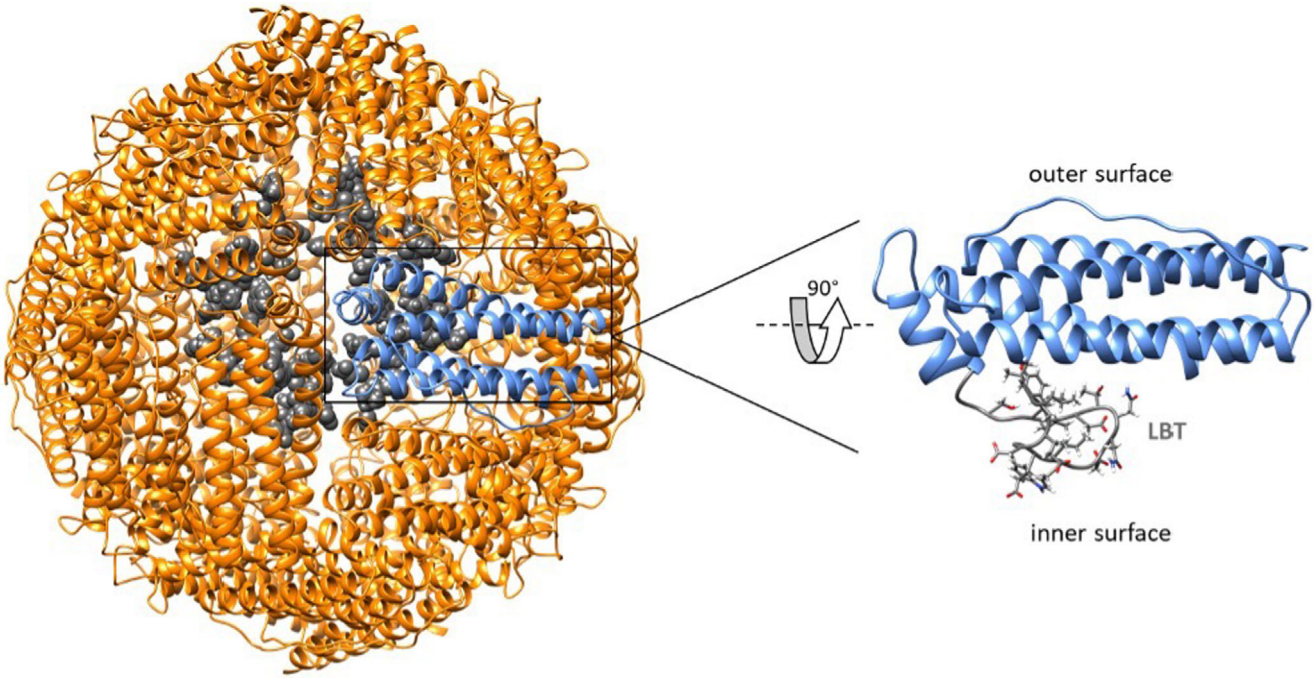

Figure 1. Structural model of HFt-LBT. On the left, the structure of the protein cage in which the LBT, pointing inside the cavity, is highlighted in gray and represented as spheres. On the right, detail of the monomer.

RESULTS

Photoluminescence of HFt-LBT Eu^{3+}

The steady-state emission properties of HFt-LBT Eu^{3+} were investigated in order to find evidence of the interaction between HFt-LBT and Eu^{3+} ions, by comparison with the optical properties of free Eu^{3+} in solution. Steady state Eu^{3+} emission spectra at different concentrations were thus recorded for comparison, by photoexciting a solution of the lanthanides dissolved in the same buffer solution at 280 nm (Fig. 2A). As expected, the emission efficiency collected from free lanthanide ions in solution was very low, as demonstrated by the signal-to-noise ratio in Fig. 2A.

Despite the low signal, it is possible to recognize several sharp spectral lines as the electronic transitions typical of europium ions. Under the same experimental conditions, the luminescence of HFt-LBT Eu^{3+} complexes, at the same lanthanides concentrations, has been recorded (Fig. 2B). Before each measurement, the samples were dialyzed with buffer (europium free) to remove unbound and weakly bound metal ions. Eu^{3+} emission efficiency was observed to be at least two orders of magnitude more intense with respect to that observed with free Eu^{3+} ions. The emission enhancement is ascribed to HFt-LBT Eu^{3+}complex formation in which Eu^{3+} is excited *via* LRET. This result is confirmed by comparing the excitation spectra of the HFt-LBT, Eu^{3+} and HFt-LBT Eu Eu^{3+} at a fixed concentration of HFt-LBT (10 μM) and Eu^{3+} (24 μM) (Figure S1). A second relevant modification is the variation of the ratio between the intensity of different electronic transitions. The $^5D_0 \rightarrow {}^7F_2$ emission line peaking at 615 nm is much more intense than the other transitions. The electric dipole (ED) $^5D_0 \rightarrow {}^7F_2$ transition is called "hypersensitive transition", which means that its intensity is more sensitive to the coordination environment around the Eu^{3+} ion, and to its geometry and symmetry, with respect to the other electronic transitions (35,36). This transition is dominant in the emission spectrum of the HFt-LBT Eu^{3+}complex, and thus primarily responsible for its high emission efficiency due to the stable chemical environment around the Eu^{3+} ion (37). The intensity ratio between the peak at 615 nm ($^5D_0 \rightarrow {}^7F_2$) and the one at 580 nm ($^5D_0 \rightarrow {}^7F_1$) is found to be 1.2 in free europium and about 4 in the HFt-LBT Eu^{3+} complexes. This variation suggests a significant modification of the Eu^{3+} local environment, corresponding to the incorporation of the ion with a consequent perturbation of its electronic transitions.

The huge increase of Eu^{3+}emission suggests that, when the complexes are formed, the UV excitation is absorbed by the protein which acts as an antenna, and then releases the energy while exciting the europium ions. The Trp are the residues involved in the protein emission (as shown in Fig. 2C), and, in particular after the photoexcitation, the Trp of the tag, which is tightly bound to the lanthanide, is expected to transfer the energy to the europium, thus increasing its emission. As a matter of fact, in order to better analyze the variations in the emission spectra of the Trp and the Eu^{3+}, and the interplay between the two, we carried out a titration by adding free Eu^{3+} ions to the HFt-LBT solution monitoring both the europium and Trp emission (Fig. 2D). The results demonstrate a progressive increase of the intensity at 615 nm for europium and an anticorrelated quenching of the Trp luminescence at 329 nm, when the Eu^{3+}/HFt-LBT concentration ratio increases. The titration endpoint, that is the Eu^{3+}/HFt-LBT ratio at which saturation is reached, was observed at two equivalent amounts of Eu^{3+} per subunit instead of the predicted one equivalent based on the presence of one LBT moiety per subunit. This suggests that the Trp residue of the LBT acts as an antenna not only for the very close Eu^{3+} ion, but also

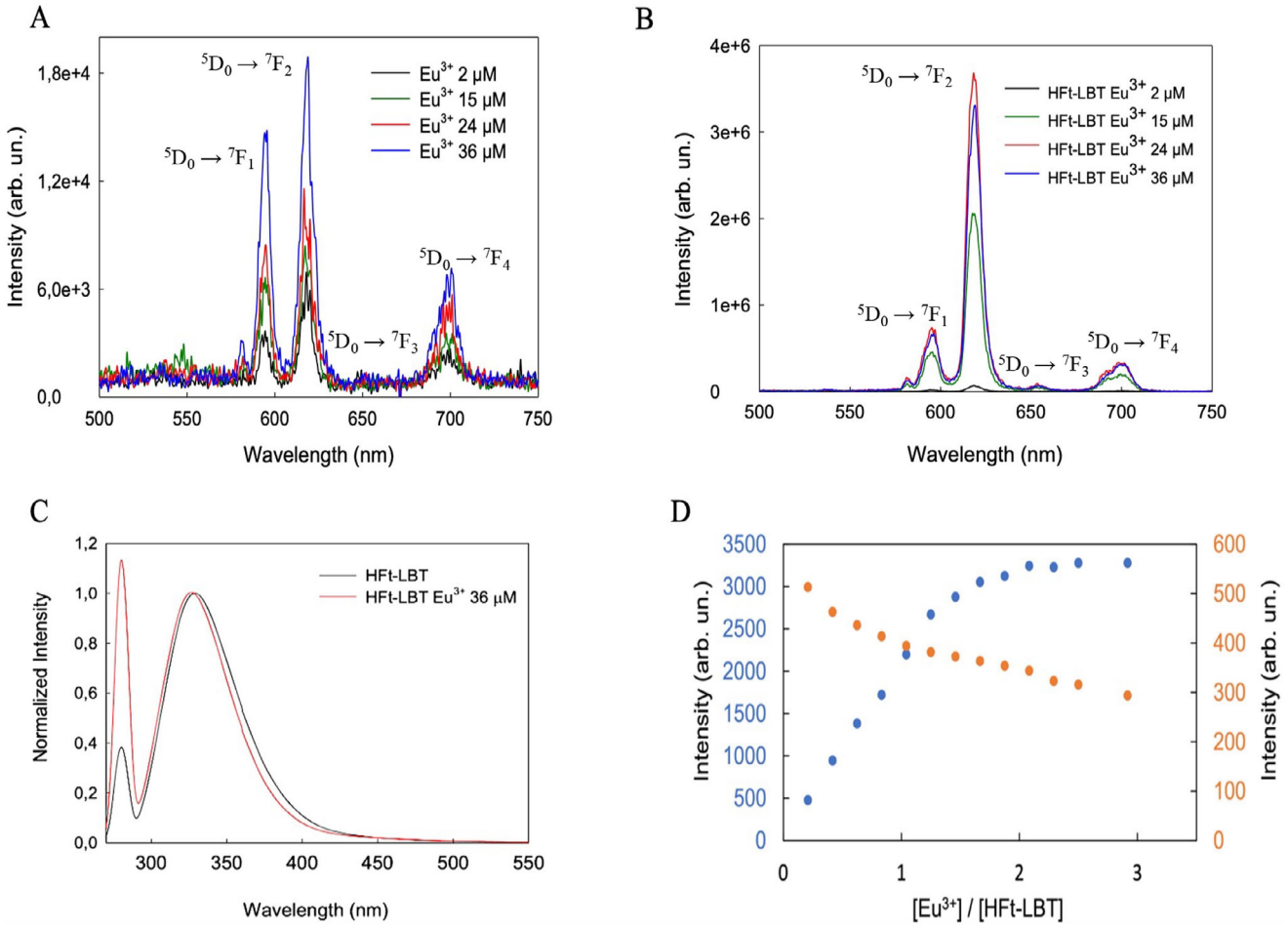

Figure 2. (A) Steady state emission spectra in the spectral range of europium emission, as excited at 280 nm of Eu^{3+} in buffer solution. (B) Steady state emission spectra in the spectral range of europium emission, as excited at 280 nm of the HFt-LBT Eu^{3+} complex, as obtained at four different concentrations of Eu^{3+}. (C) Normalized emission spectra in the near-UV of HFt-LBT and HFt-LBT Eu^{3+} complexes excited at 280 nm. (D) Luminescence intensity of HFt-LBT Eu^{3+} complex as a function of the Eu^{3+}/HFt-LBT ratio per subunit. Luminescence intensity shown in the graph was recorded at 615 nm (blue points) for the europium emission and at 329 nm (orange points) for protein emission.

for a few extra Eu^{3+} atoms bound to the natural ferritin binding sites. As reported in a previous study on HFt-LBT with terbium, the HFt-LBT construct is capable of: (1) high affinity binding of 24 Ln^{3+} atoms, one per each lanthanide binding tag; (2) intermediate affinity binding of 24 Ln^{3+} atoms at the ferroxidase binding site; and (3) lower affinity binding of 8 Ln^{3+} atoms at the entrance of the 3-fold channels (1). Hence the HFt-LBT is able to bind a total of 58 Ln^{3+} with different affinities, leading

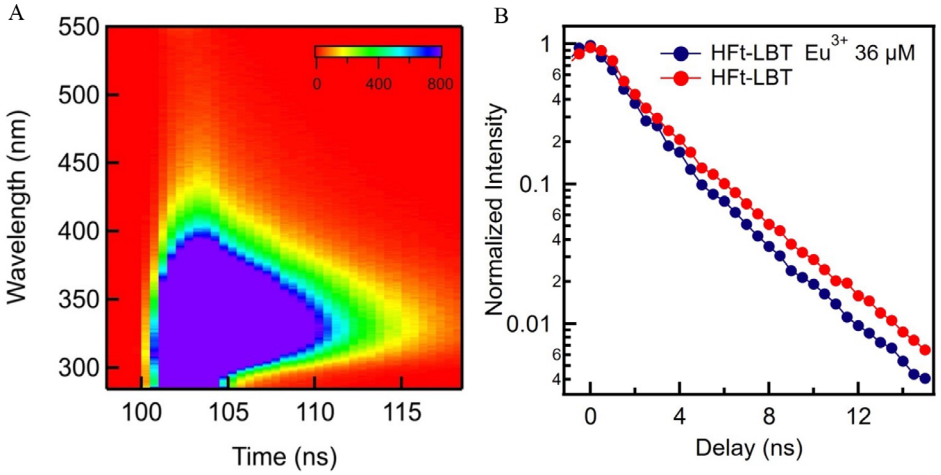

Figure 3. (A) 2D Fluorescence decay map of the HFt-LBT excited at 280 nm. (B) Kinetics decays at 340 nm of bare protein (red curve) and of HFt-LBT Eu^{3+} complex (blue curve) both excited at 280 nm.

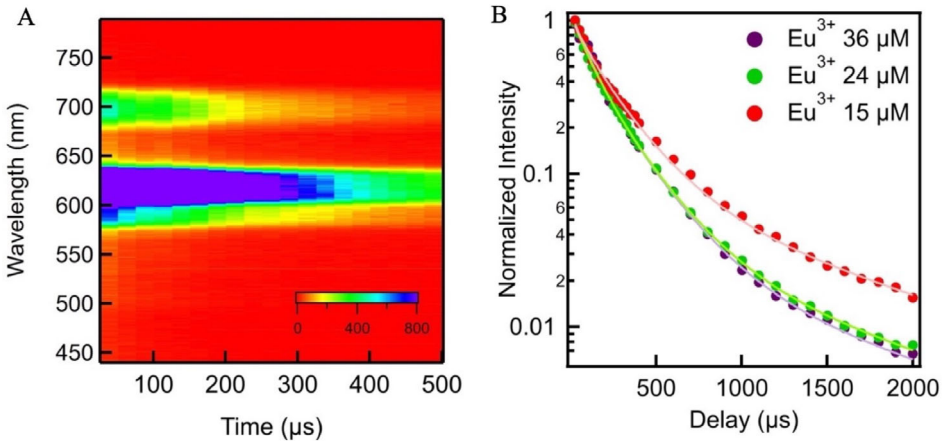

Figure 4. (A) 2D Fluorescence decay map of HFt-LBT Eu^{3+} excited at 280 nm and recorded in the visible range. (B) Decay kinetics at 615 nm of HFt-LBT Eu^{3+} complexes at three different Eu^{3+} concentrations.

to an overall stoichiometry that approaches 2.3 Ln^{3+} atoms per subunit.

In addition to the protein emission quenching, comparison of the emission spectrum of the HFt-LBT Eu^{3+} with that of bare HFt-LBT (Fig. 2C) shows a blue shift of the peak in the presence of ions due to the energy changes in the electronic transitions (38). Moreover, in order to verify the predominant involvement of Trp of the LBT with respect to other possible aromatic aminoacids, we compared the steady state emission of Eu^{3+} in contact with HFt-LBT with the one of Eu^{3+} in contact with the wild-type protein (Figure S2). From this comparison, it is evident that the other aromatic aminoacids which are contained in the protein do not have significant effects on the energy transfer process; in contrast, only the Trp within the tag is relevant for the observed enhancement.

Time-resolved photoluminescence of HFt-LBT Eu^{3+}

Time resolved measurements were carried out by recording both the emission band of the Eu^{3+} and of the Trp in order to investigate the dynamics of the energy transfer in HFt-LBT Eu^{3+}. The singlet-singlet Trp emission at 340 nm of the bare protein, excited at 280 nm, decays with a lifetime of $\tau_0 \sim 3.4$ ns as obtained by a fitting procedure from the kinetics in Fig. 3. We compared this value with the lifetime of the Trp in the HFt-LBT Eu^{3+}complex (Fig. 3B). As shown in Fig. 3B, the lifetime of the complex shortens reaching a value of $\tau_{Eu} \sim 3.0$ ns indicating an interaction between europium ions and H-Ferritin which is consistent with an energy transfer from the S_1 state of the Trp to the electronic states of Eu^{3+} (39). More precisely, from the variation of the lifetime induced by the presence of europium it is possible to directly estimate the energy transfer rate k as $\frac{1}{\tau_{Eu}} - \frac{1}{\tau_0} = 0{,}04\ ns^{-1}$.

We also analyzed the luminescence decay kinetics of the bare Eu^{3+} ions (Figure S3) and of the ions forming complexes with the HFt-LBT protein (Fig. 4). The kinetics of the $^5D_0 \rightarrow {}^7F_2$ emission at 615 nm of bare Eu^{3+} can be described as a double exponential decay with two characteristic timescales: $\tau_1 = (175 \pm 10)$ μs and $\tau_2 = (530 \pm 20)$ μs. The presence of two timescales is related to different geometrical configurations around the solvated ions in the buffer solution (40).

Table 1. Decay times τ_1 and τ_2 (and their respective weights) of the Eu^{3+}, added at three different concentrations to a solution of HFt-LBT.

	HFt-LBT Eu 15 μM	HFt-LBT Eu 24 μM	HFt-LBT Eu 36 μM
Wτ_1	26%	44%	46%
τ_1	100 ± 10 μs	100 ± 10 μs	100 ± 10 μs
Wτ_2	66%	53%	52%
τ_2	250 ± 20 μs	250 ± 20 μs	250 ± 20 μs

When europium ions bind to HFt-LBT, the recorded kinetics change and, in addition, they depend on ions concentration (Fig. 4B). The decay timescales of the 615 nm emission recorded after adding 15 μM of Eu^{3+} to the HFt-LBT solution were observed to be $\tau_1 = (100 \pm 10)$ μs and $\tau_2 = (250 \pm 20)$ μs, both values being very different from the ones observed for free Eu^{3+} in solution, thus demonstrating a binding interaction with HFt-LBT. Then, increasing the amount of europium from 15 to 24 μM we observed that the kinetics change as shown in Fig. 4B. A fitting procedure on these data indicates the presence of the same two timescales (100 μs and 250 μs) but with different weights (Table 1). Adding even more Eu^{3+} does not modify anymore the kinetics (Fig. 4B). The results of the fitting procedures on the three decay curves are reported in Table 1.

The observed changes of the kinetics with increasing europium concentration can be explained as follows. The double-exponential nature of these decay curves indicates the presence of two different protein environments corresponding to two distinct binding sites for Eu^{3+} ions. Interestingly, the amplitude of the slower kinetic component, $\tau_2 = (250 \pm 20)$ μs, is always higher than the first one, especially at the lowest concentration of added Eu^{3+}. Considering the high binding affinity between the ions and the LBT tag, it is thus reasonable to associate such a timescale to the electronic transition of europium ions which are coordinated to LBT. By contrast, the shorter phase, characterized by $\tau_1 = (100 \pm 10)$ μs, is possibly related to Eu^{3+} ions hosted within the 3-fold channels with lower binding affinity. As a control, we performed time resolved measurements on a HFt Eu^{3+} complex without the LBT. The recorded time courses are reported in Figure S3 in comparison with the tagged protein. From Figure S3C, it is evident that the kinetics are markedly different, indicating that the presence of the tag dramatically modifies the photon decay

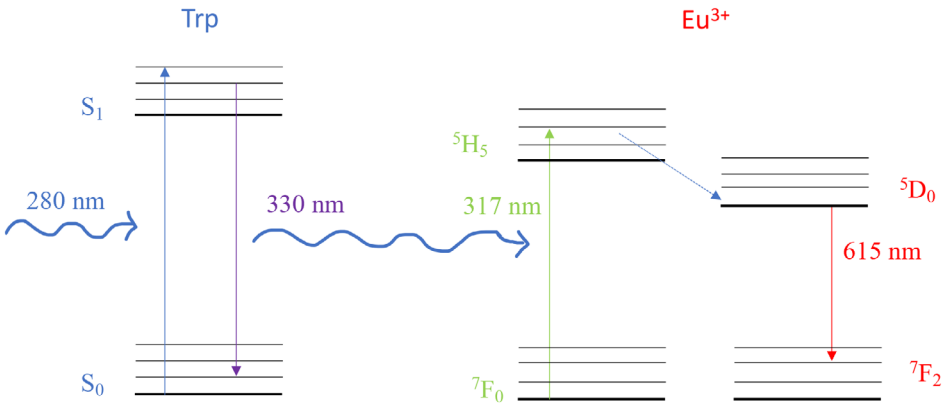

Figure 5. Schematic energy transfer process from the Trp residue of the tag to the Eu^{3+} ion in the complex HFt-LBT Eu^{3+}.

dynamics. The fitting procedure on HFt Eu^{3+} kinetics returns two rate constants $\tau_1 = (110 \pm 10)$ μs and $\tau_2 = (330 \pm 20)$ μs (Table S1). The shorter time is compatible with the shorter time obtained in presence of tag. This indicates, again, that this timescale does not depend on the tag suggesting the binding of Eu^{3+} at a site of the 3-fold channel with lower binding affinity. The longer timescale, instead, is different from that one obtained in presence of the tag, thus indicating the direct involvement of the tag in the energy transfer transition.

In order to understand which europium transition is involved in the energy transfer, we compare the absorption spectrum of the ion with the fluorescence spectrum of Trp (Figure S4). The comparison shows that the $S_1 \rightarrow S_0$ transition of Trp spectrally overlaps with several europium electronic transitions especially with the $^7F_0 \rightarrow {}^5H_5$ which most likely plays the role of the acceptor transition.

However, a classical FRET mechanism can be ruled out as being the pathway of energy transfer. In fact, from the known rate of energy transfer of 0.04 ns^{-1} which was estimated from the changes of Trp lifetime (Fig. 3), we tried to estimate the r_0 (Förster distance) (41) through the known relation $k_T(r) = \frac{1}{\tau_D}\left(\frac{R_0}{r}\right)^6$. The obtained value of $r = 0.13$ Å, is so low that it rules out a classical FRET mechanism. Besides, FRET, which is an electric dipole driven transition, is also inconsistent with the selection rules with this donor acceptor pair because the acceptor transition ($^7F_0 \rightarrow {}^5H_5$) implies a change of angular momentum higher than 1 ($\Delta J > 1$). Therefore, based on the literature, we propose that this energy transfer is a multipolar interaction between the Trp and the Eu^{3+} (42). The energy transfer is followed by a fast internal conversion to $^5D_0$ energy state which decays to $^7F_2$ emitting photons in the microsecond range. A simple model of the interaction is shown in Fig. 5.

CONCLUSIONS

A ferritin nanocage has been designed in order to guide the allocation of metal sites inside the cavity and display the best geometry for an efficient energy transfer. Thereby, mouse ferritin endowed with a specific metal binding tag, able to act as an antenna system for europium has been obtained. Energy transfer dynamics in HFt-LBT Eu^{3+} complex after photoexcitation of the antenna moiety using photoluminescence has been observed for the first time, demonstrating the successful design of a complex capable of amplifying the emission intensity of Eu^{3+} through multipolar energy transfer from Trp to the $^7F_0 \rightarrow {}^5H_5$ accepting transition of the lanthanide ions. The detailed study of the luminescent properties of the complex revealed two distinct lanthanide binding environments, one related to the specific coordination at the binding tag, and a secondary site with lower binding affinity associated to Eu^{3+} ions in the threefold channels on the protein surface. In this framework, the key physical properties of the tag are thus coupled to the CD71 receptor recognition properties of the ferritin in order to produce a unique luminescent nanovector capable of a strong emission at the typical Eu^{3+} peak at 615 nm upon Trp excitation at 280 nm. The results are very promising in view of the use of these nanomaterials in prospective theranostic applications.

Acknowledgements—The authors acknowledge the 'molecular biophysics and nanotechnologies' group and in particular Prof. Maurizio Leone for helpful suggestions and discussion.

AUTHOR CONTRIBUTIONS

Conceptualization: Valeria Militello, Alessandra Bonamore, Fabrizio Messina, Luisa Affatigato, Giuseppe Sancataldo, Alice Sciortino. Data Curation: Luisa Affatigato, Alessio Incocciati, Giuseppe Sancataldo, Alice Sciortino. Formal analysis: Luisa Affatigato, Roberta Piacentini, Giuseppe Sancataldo, Alice Sciortino. Funding Acquisition: Alessandra Bonamore, Valeria Militello, Mariano Licciardi, Marco Cannas. Methodology: Luisa Affatigato, Alessio Incocciati, Alice Sciortino. Project Administration: Valeria Militello. Supervision: Alessandra Bonamore, Fabrizio Messina, Valeria Militello. Writing – Original draft: Luisa Affatigato, Alice Sciortino. Writing – review & editing: Alessandra Bonamore, Mariano Licciardi, Marco Cannas, Fabrizio Messina, Valeria Militello.

SUPPORTING INFORMATION

Additional supporting information may be found online in the Supporting Information section at the end of the article:

Figure S1. Excitation spectra of HFt-LBT, $Eu^{3+}$and HFt-LBT Eu^{3+}.The emission wavelength is 615 nm.

Figure S2. (A) Steady state emission spectra in the spectral range of Europium emission, as excited at 280 nm of Eu^{3+} in complex with HFt and in complex with HFt-LBT.

Figure S3. (A) 2D Fluorescence decay map of the Eu^{3+} excited at 280 nm. (B) Luminescence decay of Eu^{3+} in buffer

solution. (C) Luminescence decay of Eu^{3+} in complex with HFt and with HFt-LBT.

Figure S4. Overlapping of the emission spectrum of HFt-LBT (λ_{exc} = 280 nm) and the absorbance spectrum of Eu^{3+}.

Table S1. Luminescence decay times τ_1 and τ_2 of Eu^{3+} in buffer solution, in complex with HFt and in complex with HFt-LBT.

REFERENCES

1. Calisti, L., M. C. Trabuco, A. Boffi, C. Testi, L. C. Montemiglio, A. Des Georges, A. Des Georges, I. Benni, A. Ilari, B. Taciak, M. Bialasek, T. Rygiel, M. Krol, P. Baiocco and A. Bonamore (2018) Engineered ferritin for lanthanide binding. *PLoS One* **13**, 13.
2. Palombarini, F., E. Fabio, A. Boffi, A. Macone and A. Bonamore (2020) Ferritin nanocages for protein delivery to tumor cells. *Molecules* **25**(4), 825.
3. Macone, A., S. Masciarelli, F. Palombarini, D. Quaglio, A. Boffi, M. C. Trabuco, P. Baiocco, F. Fazi and A. Bonamore (2019) Ferritin nanovehicle for targeted delivery of cytochrome C to cancer cells. *Sci. Rep.* **9**, 11749.
4. Ferrari, M. (2005) Cancer nanotechnology: Opportunities and challenges. *Nat. Rev. Cancer* **5**, 161–171.
5. Blanco, E., H. Shen and M. Ferrari (2015) Principles of nanoparticle design for overcoming biological barriers to drug delivery. *Nat. Biotechnol.* **33**, 941–951.
6. Tesarova, B., K. Musilek, S. Rex and Z. Heger (2020) Taking advantage of cellular uptake of ferritin nanocages for targeted drug delivery. *J. Control. Rel.* **325**, 176–190.
7. Bellini, M., S. Mazzucchelli, E. Galbiati, S. Sommaruga, L. Fiandra, M. Truffi, M. A. Rizzuto, M. Colombo, P. Tortora, F. Corsi and D. Prosperi (2014) Protein nanocages for self-triggered nuclear delivery of DNA-targeted chemotherapeutics in cancer cells. *J. Control. Release* **196**, 184–196.
8. He, J., K. Fan and X. Yan (2019) Ferritin drug carrier (FDC) for tumor targeting therapy. *J. Control. Rel.* **311-312**, 288–300.
9. Fracasso, G., E. Falvo, G. Colotti, F. Fazi, T. Ingegnere, A. Amalfitano, G. V. Doglietto, S. Alfieri, A. Boffi, V. Morea, G. Conti, E. Tremante, P. Giacomini, A. Arcovito and P. Ceci (2016) Selective delivery of doxorubicin by novel stimuli-sensitive nano-ferritins overcomes tumor refractoriness. *J. Control. Release* **239**, 10–18.
10. Li, L., C. J. Fang, J. C. Ryan, E. C. Niemi, J. A. Lebrón, P. J. Björkman, H. Arase, F. M. Torti, S. V. Torti, M. C. Nakamura and W. E. Seaman (2010) Binding and uptake of H-ferritin are mediated by human transferrin receptor-1. *Proc. Natl. Acad. Sci. USA* **107**, 3505–3510.
11. Fan, K., C. Cao, Y. Pan, D. Lu, D. Yang, J. Feng, L. Song, M. Liang and X. Yan (2012) Magnetoferritin nanoparticles for targeting and visualizing tumour tissues. *Nat. Nanotechnol.* **7**, 459–464.
12. Arosio, P., L. Elia and P. M. Ferritin (2017) Cellular iron storage and regulation. *IUBMB Life* **69**, 414–422.
13. Theil, E. C., T. Tosha and R. K. Behera (2016) Solving Biologys iron chemistry problem with ferritin protein Nanocages. *Acc. Chem. Res.* **49**, 784–791.
14. Bou-Abdallah, F. (2010) The iron redox and hydrolysis chemistry of the ferritins. *Biochim. Biophys. Acta Gen. Subj.* **1800**, 719–731.
15. Honarmand Ebrahimi, K., P. L. Hagedoorn and W. R. Hagen (2015) Unity in the biochemistry of the iron-storage proteins ferritin and bacterioferritin. *Chem. Rev.* **115**, 295–326.
16. Calisti, L., I. Benni, M. Cardoso Trabuco, P. Baiocco, B. Ruzicka, A. Boffi, E. Falvo, F. Malatesta and A. Bonamore (2017) Probing bulky ligand entry in engineered archaeal ferritins. *Biochim. Biophys. Acta Gen. Subj.* **1861**, 450–456.
17. Zhen, Z., W. Tang, H. Chen, X. Lin, T. Todd, G. Wang, T. Cowger, X. Chen and J. Xie (2013) RGD-modified apoferritin nanoparticles for efficient drug delivery to tumors. *ACS Nano* **7**, 4830–4837.
18. Kanekiyo, M., C. J. Wei, H. M. Yassine, P. M. McTamney, J. C. Boyington, J. R. R. Whittle, S. S. Rao, W. P. Kong, L. Wang and G. J. Nabel (2013) Self-assembling influenza nanoparticle vaccines elicit broadly neutralizing H1N1 antibodies. *Nature* **499**, 102–106.
19. Wang, Z., H. Gao, Y. Zhang, G. Liu, G. Niu and X. Chen (2017) Functional ferritin nanoparticles for biomedical applications. *Front. Chem. Sci. Eng.* **11**, 633–646.
20. Bain, J. and S. S. Staniland (2015) Bioinspired nanoreactors for the biomineralisation of metallic-based nanoparticles for nanomedicine. *Phys. Chem. Chemical Phys.* **17**, 15508–15521.
21. Maity, B., S. Abe and T. Ueno (2017) Observation of gold sub-nanocluster nucleation within a crystalline protein cage. *Nat. Commun.* **8**, 14820.
22. Handl, H. L. and R. J. Gillies (2005) Lanthanide-based luminescent assays for ligand-receptor interactions. *Life Sci.* **77**, 361–371.
23. Bao, G. (2020) Lanthanide complexes for drug delivery and therapeutics. *J. Luminescence* **228**, 117622.
24. Bünzli, J. C. G. (2006) Benefiting from the unique properties of lanthanide ions. *Acc. Chem. Res.* **39**, 53–61.
25. Hemmilä, I. and V. Laitala (2005) Progress in lanthanides as luminescent probes. *J. Fluoresc.* **4**, 529–542.
26. Richardson, F. S. (1982) Terbium(III) and europium(III) ions as luminescent probes and stains for biomolecular systems. *Chem. Rev.* **82**, 541–552.
27. Yang, C., L. M. Fu, Y. Wang, J. P. Zhang, W. T. Wong, X. C. Ai, Y. F. Qiao, B. S. Zou and L. L. Gui (2004) A highly luminescent europium complex showing visible-light-sensitized red emission: Direct observation of the singlet pathway. *Angew. Chem. Int. Ed.* **38**, 5010–5013.
28. Silly, M. G., S. Blanchandin, F. Sirotti, F. Lux, S. Chevreux, G. Lemercier and F. Charra (2013) Evidence of mixed-valence hydrated europium-chloride phase in vacuum by means of optical and electronic spectroscopies. *J. Phys. Chem. C* **19**, 9766–9771.
29. Sculimbrene, B. R. and B. Imperiali (2006) Lanthanide-binding tags as luminescent probes for studying protein interactions. *J. Am. Chem. Soc.* **22**, 7346–7352.
30. Huang, Y. J., C. Ke, L. M. Fu, Y. Li, S. F. Wang, Y. C. Ma, J. P. Zhang and Y. Wang (2019) Excitation energy-transfer processes in the sensitization luminescence of europium in a highly luminescent complex. *Chemistry Open* **3**, 388–392.
31. Bünzli, J. C. G. and S. V. Eliseeva (2010) *Basics of Lanthanide Photophysics*, Vol. **VII**. p. 45. Springer Series on fluorescence book series (SS FLUOR). Springer, Berlin, Heidelberg.
32. Kido, J. and Y. Okamoto (2002) Organo lanthanide metal complexes for electroluminescent materials. *Chem. Rev.* **6**, 2357–2368.
33. Aulsebrook, M. L., B. Graham, M. R. Grace and K. L. Tuck (2018) Lanthanide complexes for luminescence-based sensing of low molecular weight analytes. *Coordination Chem. Rev.* **375**, 191–220.
34. Martin, L. J., M. J. Hähnke, M. Nitz, J. Wöhnert, N. R. Silvaggi, K. N. Allen, H. Schwalbe and B. Imperiali (2007) Double-lanthanide-binding tags: Design, photophysical properties, and NMR applications. *J. Am. Chem. Soc.* **22**, 7106–7113.
35. Choppin, G. R. and D. R. Peterman (1998) Applications of lanthanide luminescence spectroscopy to solution studies of coordination chemistry. *Coord. Chem. Rev.* **174**, 283–299.
36. Heffern, M. C., L. M. Matosziuk and T. J. Meade (2014) Lanthanide probes for bioresponsive imaging. *Chem. Rev.* **114**, 4496–4539.
37. Binnemans, K. (2015) Interpretation of europium(III) spectra. *Coordination Chem. Rev.* **295**, 1–45.
38. Sindrewicz, P., X. Li, E. A. Yates, J. E. Turnbull, L. Y. Lian and L. G. Yu (2019) Intrinsic tryptophan fluorescence spectroscopy reliably determines galectin-ligand interactions. *Sci. Rep.* **9**(1), 1–12.
39. Miyazaki, S., K. Miyata, H. Sakamoto, F. Suzue, Y. Kitagawa, Y. Hasegawa and K. Onda (2020) Dual energy transfer pathways from an antenna ligand to lanthanide ion in trivalent europium complexes with phosphine-oxide bridges. *J. Phys. Chem.* **33**, 6601–6606.
40. Bünzli, J. C. G., A. S. Chauvin, H. K. Kim, E. Deiters and S. Eliseeva (2010) Lanthanide luminescence efficiency in eight- and nine-coordinate complexes: Role of the radiative lifetime. *Coord. Chem. Rev.* **254**, 2623–2633.
41. Lakowicz, J. R. (2006) *Principles of Fluorescence Spectroscopy*, p. 954. Springer, New York.
42. Tanner, P. A., L. Zhou, C. Duan and K. L. Wong (2018) Misconceptions in electronic energy transfer: Bridging the gap between chemistry and physics. *Chem. Soc. Rev.* **14**, 5234–5265.